International Journal of Chemical, Materials and Biomolecular Sciences
ISSN: 2415-6620
Vol:5, No:7, 2011

Efficiency Improvements of GaAs-based Solar Cells by Hydrothermally-deposited ZnO Nanostructure Array

Chun-Yuan Huang, Chiao-Yang Cheng, Chun-Yem Huang, Yan-Kuin Su, and James Chin-Lung Fang

***Abstract*—**ZnO nanostructures including nanowires, nanorods, and nanoneedles were successfully deposited on GaAs substrates, respectively, by simple two-step chemical method for the first time. A ZnO seed layer was firstly pre-coated on the O_2-plasma treated substrate by sol-gel process, followed by the nucleation of ZnO nanostructures through hydrothermal synthesis. Nanostructures with different average diameter (15-250 nm), length (0.9-1.8 μm), density ($0.9\text{-}16\times10^9$ cm^{-2}) were obtained via adjusting the growth time and concentration of precursors. From the reflectivity spectra, we concluded ordered and taper nanostructures were preferential for photovoltaic applications. ZnO nanoneedles with an average diameter of 106 nm, a moderate length of 2.4 μm, and the density of 7.2×10^9 cm^{-2} could be synthesized in the concentration of 0.04 M for 18 h. Integrated with the nanoneedle array, the power conversion efficiency of single junction solar cell was increased from 7.3 to 12.2%, corresponding to a 67% improvement.

***Keywords*—**Anti-reflection, Chemical synthesis, Solar cells, ZnO nanostructures.

I. Introduction

AS a functional material with unique optical and electrical properties, zinc oxide (ZnO) has attracted worldwide attention for its novel applications on electronic and optoelectronic devices [1]-[3]. For instance, ZnO films with the exciton binding energy of 60 meV and a tunable bandgap energy have been a promising candidate to replace GaN for UV and visible light-emitting diodes [3], [4]. With high piezoelectric coupling coefficients, ZnO can be used for making low-loss surface acoustic wave (SAW) filters operating at high frequencies [5]. In particular, numerous types of one-dimensional nanostructures grown by physical or chemical routes indicate that this material should be the richest family of nanostructures [6], besides the ordinary ZnO film deposition. Through precisely controlling the growth kinetics and local temperature, diverse and highly pure nanostructures with different crystallinity, crystallographic orientation, crystallite size, morphology, geometry, and distribution density can be obtained. Since these nanostructures typically play an auxiliary role to boost inherent properties of devices and to benefit their commercializing, reliable and economic deposition techniques for the attachment of large-scale ZnO nanostructures is the most essential requirement [7]. In fact, many kinds of crystalline ZnO nanostructures have been demonstrated to be deposited on silicon, GaN, GaP, glass, indium tin oxide (ITO), and flexible substrates like poly(ethylene terephthalate) (PET) and polydimethylsiloxane (PDMS), by cost-effective methods such as hydrothermal synthesis [7]-[12].

Being a representative second-generation semiconductor material, gallium arsenide has seldom been reported to merge with ZnO nanostructures. As for those successfully grown, all were via expensive deposition equipment such as metal-organic chemical vapor deposition (MOCVD) or molecular beam epitaxy (MBE), which was not beneficial for reducing the fabrication cost [13], [14]. Here, for the first time, high quality ZnO nanostructures were deposited on GaAs substrates precoated with a ZnO seed layer for nucleation by simple hydrothermal synthesis [10]. Nanowire, nanorod, and nanoneedle arrays can be archieved by adjusting the growth time and the concentration of precursors, respectively. Further integration of highly-ordered nanoneedle arrays on GaAs-based solar cells has significantly increased the device performances.

II. Experimental Details

Two-step growh was adopted in the present study. The solution for ZnO seed layer was firstly prepared by sol-gel process prior to the growth of ZnO nanostructures via additive-free hydrothermal synthesis [15]. The ZnO sol-gel was formed as follows: 1g zinc acetate was added in 10 ml absolute ethanol and the solution was stirred at 80 ℃ for 30 minutes, in which 1 ml distilled water was added and stirred for 5 minutes. To provide sufficient wettability, the GaAs substrates were pre-treated with O_2 plasma [16]. A polycrystalline ZnO seed layer with controlled thickness of 80 nm was then obtained by spin-casting the gelled solution on pre-cleaned GaAs substrates and subsequently annealing at various temperatures. The seed-layer/GaAs substrates were then mounted on a glass slide and then soaked in aqueous solution of zinc acetate dihydrate [$Zn(OAc)_2\cdot\ 2H_2O$] and hexamethylenetetramine (HMTA), the

The authors are grateful to the National Science Council of the Republic of China, Taiwan, for funding this research under contract no. NSC 99 - 2221 - E - 143 - 002.

C.-Y. Huang is with the Department of Applied Science, National Taitung University, Taitung 950, Taiwan (phone: +886-89-356516; fax: +886-89-517316; e-mail: laputa@nttu.edu.tw).

C.-Y. Cheng and J. C.-L. Fang are with the Wafer Works Optronics Corp., Chung-Li, Taoyuan, Taiwan.

Y.-K. Su is with the Institute of Microelectronics, Department of Electrical Engineering, National Cheng Kung University, Tainan 701, Taiwan.

precursors, in a bottle with an autoclavable screw cap. Inside a conventional laboratory oven, the sealed bottle was baked at 90 ℃ for 1, 3, 5, and 18 h, while the concentration of both $Zn(OAc)_2 \cdot 2H_2O$ and HMTA in mixed solution was varied as 0.01, 0.02, 0.03, 0.04, and 0.05 M, respectively. No extra catalysts such as polyethylene glycol (PEG) or polyvinyl pyrrolidone (PVP) were utilized during the whole process. After reaction, the samples were washed repeatedly with deionized water and blow-dried with N_2 gas for characterization. Thereby, the synthesized nanostructures were evaluated by scanning electron microscopy (SEM) and the reflectivity of these ZnO nanostructures on GaAs substrates was measured.

The fabrication process of single junction solar cells (SCs) was as introduced in previous report [15]. Au/Ge/Ni and Au/Zn were evaporated and annealing at 425 ℃ as the back and front contact, respectively. As the anti-reflection (AR) layer, ZnO nanostructure arrays were grown on the front surface of SCs according to the observations in the growth of ZnO nanostructure arrays. The phase composition and crystallinity of samples was characterized using X-ray diffraction (XRD). A Keithley 2400 sourcemeter was used to measure current density-voltage (*J-V*) characteristics of the SCs. The illumination was calibrated by the calibration cell of NREL with a known one-sun AM1.5G short-circuit current value.

III. Results and Discussion

Fig. 1 shows the XRD spectra of ZnO seed layers annealed at 130, 200, 300, and 500 ℃, respectively, with the result of seed layer as-deposited. As shown, the films were polycrystalline, well-defined diffraction peaks corresponding to the crystalline orientations, (100), (002), and (101), of ZnO wurtzite structure were observed. Low peak intensities should be attributed to the amorphous phase in films, which was confirmed from the amorphous seed layer before annealing. In contrast to the results previously reported [17], the raise of annealing temperature did not improve the crystalline quality, nor was preferential growth orientation observed despite the temperature. However, from the optical microscopy (OM) photographs (not shown), too high a temperature has led to the cracks of ZnO films due to the discrepancy of thermal expansion between ZnO thin film and GaAs substrate [18]. Crack-free and smooth surface was only observed on the seed layer annealed at 130 ℃, which was used for the following growth of nanostructures.

Fig. 2 and Fig. 3 show SEM photographs of geometry and distribution of ZnO nanostructures grown in 0.01 M solution for different growth time, and different concentration for 1 hour, respectively. For better understanding the variations, statistics results including average diameter, length, and density, are shown in Fig. 4. The densities of nanostructures were basically calculated from the top view images. It should be mentioned, however, densities of randomly-oriented

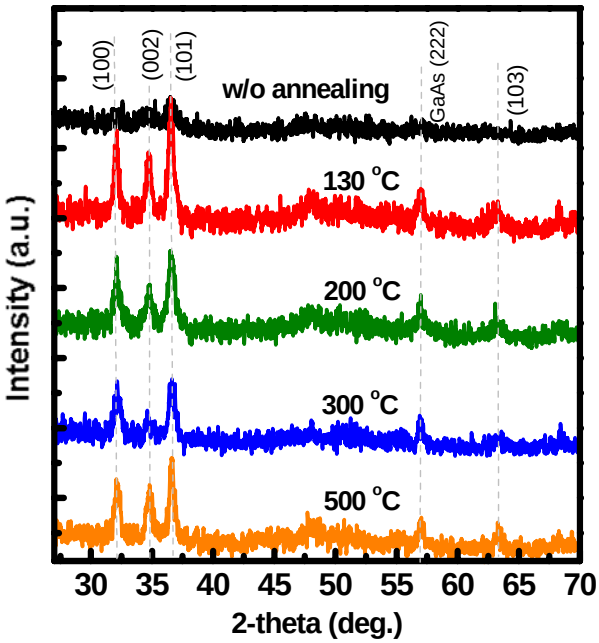

Fig. 1 XRD spectra of sol-gel deposited ZnO seed layers annealed at 150, 200, 300, and 500 ℃, respectively. Also shown is the result of as-deposited one for reference.

nanostructures could be underestimated due to the untraceable overlap. The wire distribution was very homogeneous on the whole substrate. Initially (Figs. 2(a) and 2(b)), wires were grown with diameters ranging between 10–20 nm and length of 980 nm, and with a number density of 1.6×10^{10} cm^{-2}. As previous reports, multiple nanowires were frequently grown from a single cluster, only a portion of nanowires can vertically develop and others were inclined toward any directions. Since the cluster is directly related to the crystal size of seed layer and

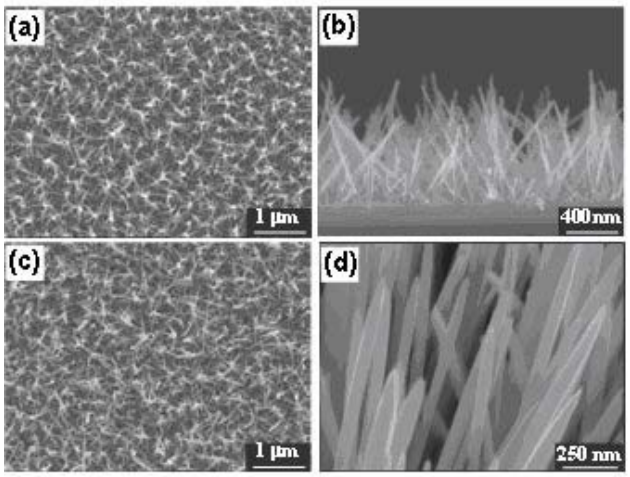

Fig. 2 SEM photographs of ZnO nanowire arrays prepared in the 0.01 M solution for (a,b) 1 and (c,d) 18 hours, respectively.

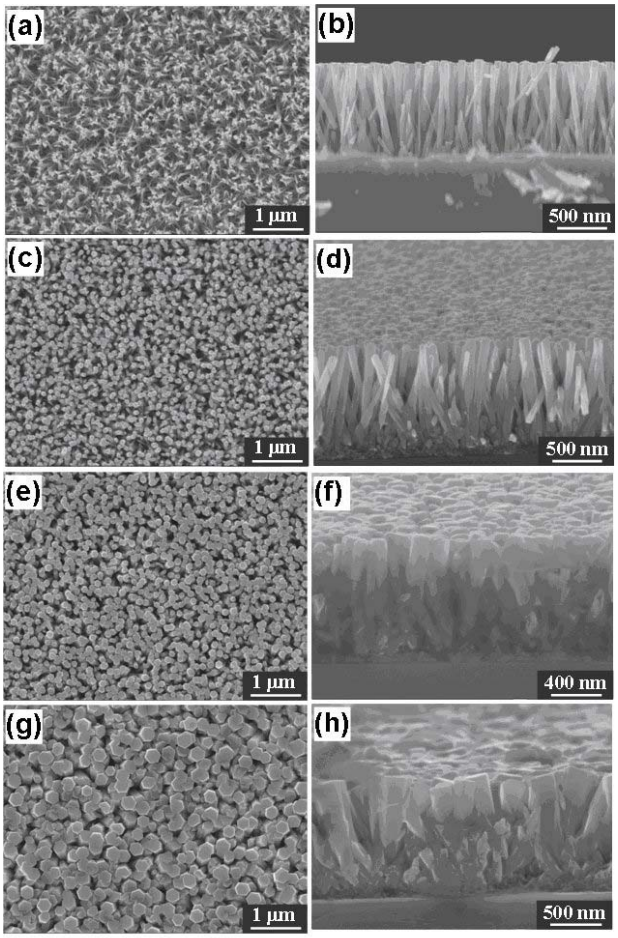

Fig. 3 SEM photographs of ZnO nanowire and nanorod arrays grown in the precursor concentration of (a,b) 0.01, (c,d) 0.03, and (e,f) 0.05 M, respectively.

oriented ZnO nanowires are preferentially grown on oriented seed layer, low alignment ordering of nanowire at the beginning stage should be attributed to the seed layer's polycrystal nature and overripened crystal size inferred from XRD pattern [19]. The average size of these nanostructures increased with prolonging the growth time, however, the increase was not significant. Actually, the aspect ratio of nanowires grown from 1 to 18 hours did not change very much. In contrast, the nanowires transformed to be nanorods with a diameter between 130 to 230 nm with the concentration increasing in Fig. 3. Consequently, those misaligned nanorods from adjacent clusters gradually impinged on one another and were forced to grow along the same direction. From the hexagonal ends of rods, we can confirm that the vertical growth direction is c-axis direction. Some close-contacted individuals began to merge together and thus increased the divergence of rod width and decrease the rod density. At this stage, all nanorods were gradually vertically aligned because of the close pack effect. The favored c-axis growth direction has been interpreted by the higher surface energy of polar *c*-plane. The flattened wire top was attributed to the etching (dissolution)

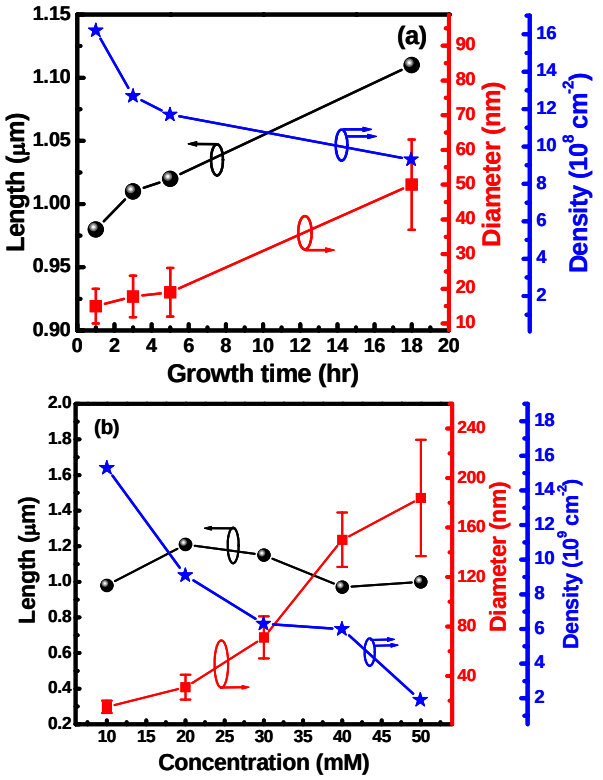

Fig. 4 Plots of average length and diameter of nanostructures as a function of (a) growth time and (b) concentration of precursors, respectively. The solid lines are drawn for eye guidance.

effect, since the formation and dissolution of ZnO nanostructures were simultaneously happened at different rates [20]. On the other hand, due to the critical diffusion of monomers and the limited nucleation free energy, the average diameter of nanowires was proportional to the concentration of chemical precursors and could be increased one order of magnitude from 15 to 180 nm. This enables us to manipulate the concentration to obtain appropriate diameters of nanostructures. Interestingly, more and more nanorods became tapered when the concentration was increased. As a result, separated nanorods were observed in top-view photographs while nearly all of adjacent nanorods were merged together at their bases in side-view ones. The taper effect gave us a hint about the nanoneedle array observed in Fig. 2(d). Taper-shaped nanorods eventually evolved to be directional nanoneedles after long time deposition. It can be attributed to that the decrease (consuming) of Zn^{2+} concentration during the reaction should affect the broadening of nanostructures. As a result, the significant decrease of Zn^{2+} concentration reflected on the tapering of nanostructures along the vertical direction.

To be the AR layer, the reflectivity spectra of above ZnO nanostructure arrays were characterized. As shown in Fig. 5, the nanowire array grown in 0.01 M exhibited very low reflectivity at long wavelength range. We believed that the decrease of reflectivity should be from the light scattering caused by disordered nanowire distribution (Fig. 2(a)), instead

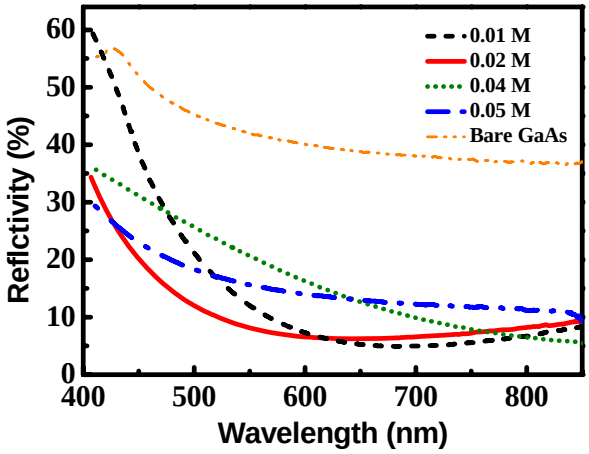

Fig. 5 Reflectivities of ZnO nanostructures on GaAs substrates. Also shown is the reflectivity of bare GaAs substrate for comparison.

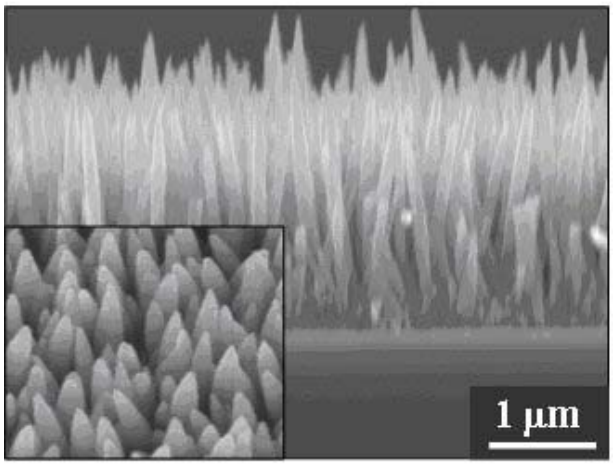

Fig. 6 SEM photograph of ZnO nanoneedle array grown in the precursor concentration of 0.02 M for 18 hours on designed SCs.

of the increase of transmittance. We also noted the reflectivity may be increased with the nanorod diameter, which may be attributed to the large and flat top surface of rods originated from large diameters. According to the SEM and reflectivity results, we concluded that ordered nanoneedle arrays with less rod-coalescence could be obtained from the long time growth in precursor concentration of 0.02 M, likewise. The SEM photographs shown in Fig. 6 exhibited that highly-ordered and vertically-oriented ZnO nanoneedle arrays were with an average diameter of 106 nm, a moderate length of 2.4 μm, and the density of 7.2×10^9 cm^{-2}. The current density-voltage (*J-V*) curves and incident photon-to-current efficiency (IPCE) spectra of SCs with and without the nanoneedle array are shown in Fig. 7. Due to the increase of incident light intensity by attaching the nanoneedle array, the short-circuit current density (J_{sc}) was increased from 12.75 to 18.46 mA/cm^2. In addition, it turned to be the increase of power conversion efficiency (PCE) from 7.3 to 12.2%, which corresponded to a

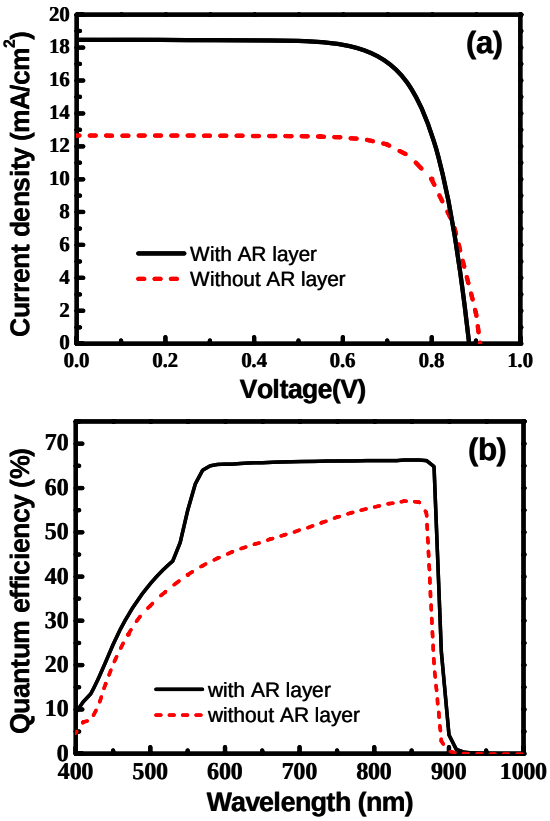

Fig. 7 (a) *J-V* curves and (b) IPCE spectra of designed SCs with and without the nanoneedle array shown in Fig. 6.

67% improvement. If we take into account the solar spectrum and define the solar-weighted reflectance (SWR) as [21]:

$$SWR = \frac{\int_{300\ nm}^{850\ nm} \frac{R_s(\lambda)SI(\lambda)}{E(\lambda)} d\lambda}{\int_{300\ nm}^{850\ nm} \frac{SI(\lambda)}{E(\lambda)} d\lambda} \quad (1)$$

where $SI(\lambda)$ is the spectral irradiance, $R_s(\lambda)$ the real reflectivity spectrum, and $E(\lambda)$ the photon energy, respectively. A reflectance (SWR) of 12% can be calculated for our ordered nanoneedle array over the entire spectral region. With this demonstration, it provides the direct evidence that the decrease of the reflectivity of GaAs substrates with nanostructure array attached is mainly due to the increase of light absorption, instead of the light scattering.

IV. Conclusion

In conclusion, ZnO nanostructures were demonstrated to be deposited on GaAs substrates by cost-effective two-step process for the first time. The spin-coating and annealing procedures of ZnO seed layer prepared by sol-gel process played a determinative role in the following

hydrothermally-synthesized ZnO nanostructures. With the growth time prolonging, the nanostructures could evolve to be nanowires, nanorods, and finally nanoneedles. Through the proper manipulation of the precursor concentration and growth time, highly-ordered and vertically oriented nanoneedles could be successfully integrated to GaAs-based single junction solar cells, which enabled the power conversion efficiency to be significantly boosted from 7.3 to 12.2%.

REFERENCES

[1] R. L. Hoffman, B. J. Norris, and J. F. Wager, "ZnO-based transparent thin-film transistors," *Appl. Phys. Lett.*, vol. 82, pp. 733-735, 2003
[2] J. Schrier, D. O. Demchenko, and L. W. Wang, "Optical properties of ZnO/ZnS and ZnO/ZnTe heterostructures for photovoltaic applications," *Nano Lett.*, vol. 7, pp. 2377-2381, 2007.
[3] A. Tsukazaki,; A. Ohtomo, T. Onuma,; M. Ohtani, T. Makino, M. Sumiya, K. Ohtani, S. F. Chichibu, S. Fuke, Y. Segawa, H. Ohno, H. Koinuma, and M. Kawasaki, "Repeated temperature modulation epitaxy for p-type doping and light-emitting diode based on ZnO," *Nat. Mater.*, vol. 4, pp. 42-45, 2005.
[4] L. J. Mandalapu, Z. Yang, S. Chu, and J. L. Liu, "Ultraviolet emission from Sb-doped p-type ZnO based heterojunction light-emitting diodes," *Appl. Phys. Lett.*, vol. 92, pp. 122101 1-3, 2008.
[5] J. B. Lee, M. H. Lee, C. K. Park, and J. S. Park, "Effects of lattice mismatches in ZnO/substrate structures on the orientations of ZnO films and characteristics of SAW devices," *Thin Solid Films*, vol. 447, pp. 296-300, 2004.
[6] S. Kar, B. N. Pal, S. Chaudhuri, and D. Chakravorty, "One-dimensional ZnO nanostructure arrays: synthesis and characterization," *J. Phys. Chem. B*, vol. 110, pp. 4605-4608, 2006.
[7] Y. Gao and M. Nagai, "Morphology evolution of ZnO thin films from aqueous solutions and their application to solar cells," *Langmuir*, vol. 22, pp. 3936-3939, 2006.
[8] X. M. Zhang, M. Y. Lu, Y. Zhang, L. J. Chen, and Z. L. Wang, "Fabrication of a high- brightness blue- light- emitting diode using a ZnO- nanowire array grown on p-GaN thin film," *Adv. Mater.*, vol. 21, pp. 2767-2770, 2009.
[9] S. S. Shinde, P. S. Patil, R. S. Gaikwad, R. S. Mane, B. N. Pawar, and K. Y. Rajpure, "Influences in high quality zinc oxide films and their photoelectrochemical performance," *J. Alloy Compd.*, vol. 503, pp. 416-418, 2010.
[10] J. X. Wang, X. W. Sun, Y. Yang, H. Huang, Y. C. Lee, O. K. Tan, and L. Vayssieres, "Hydrothermally grown oriented ZnO nanorod arrays for gas sensing applications," *Nanotechnol.*, vol. 17, pp. 4995-4998, 2006.
[11] B. Weintraub, Y. Deng, and Z. L. Wang, "Position-controlled seedless growth of ZnO nanorod arrays on a polymer substrate via wet chemical synthesis," *J. Phys. Chem. C*, vol. 111, pp. 10162-10165, 2007.
[12] Y. K. Su, S. M. Peng, L. W. Ji, C. Z. Wu, W. B. Cheng, and C. H. Liu, "Ultraviolet ZnO nanorod photosensors," *Langmuir*, vol. 26, pp. 603-606, 2010.
[13] W. Lee, M. C. Jeong, and J. M. Myoung, "Ultraviolet electroluminescence from controlled arsenic-doped ZnO nanowire homojunctions," *Nanotechnol.*, vol. 15, vol. 254-257, 2004.
[14] Y. W. Heo, M. Kaufman, K. Pruessner, K. N. Siebein, D. P. Norton, and F. Ren, "ZnO/cubic (Mg, Zn) O radial nanowire heterostructures," *Appl. Phys. A*, vol. 80, pp. 263-266, 2005.
[15] B. Y. Su, Y. K. Su, Z. L. Tseng, M. F. Shih, C. Y. Cheng, T. H. Wu, C. S. Wu, J. J. Yeh, P. Y. Ho, Y. D. Juang, and S. Y. Chu, "Antireflective and radiation resistant ZnO thin films for the efficiency enhancement of GaAs photovoltaics," *J. Electrochem. Soc.*, vol. 158, pp. H267-H270, 2011.
[16] C. Y. Cheng, F. C. N. Hong, and C. Y. Huang, "Micro-and nanopatterned polymethylmethacrylate layers on plastic poly (ethylene terephthalate) substrates by modified roller-reversal imprint process," *J. Vac. Sci. Technol. B*, vol. 28, pp. 921-925, 2010.
[17] R. Ghosh, G. K. Paul, and D. Basak, "Effect of thermal annealing treatment on structural, electrical and optical properties of transparent sol-gel ZnO thin films," *Mater. Res. Bull.*, vol. 40, pp. 1905-1908, 2005.
[18] A. Wei, X. W. Sun, C. X. Xu, Z. L. Dong, Y. Yang, S. T. Tan, and W. Huang, "Growth mechanism of tubular ZnO formed in aqueous solution," *Nanotechnol.*, vol. 17, pp. 1740-1744, 2006.
[19] M. Guo, P. Diao, and S. Cai, "Hydrothermal growth of well-aligned ZnO nanorod arrays: Dependence of morphology and alignment ordering upon preparing conditions," *J. Solid State Chem.*, vol. 178, pp. 1864-1867, 2005.
[20] L. E. Greene, M. Law, J. Goldberger, F. Kim, J. C. Johnson, Y. Zhang, R. J. Saykally, and P. Yang, "Low-temperature wafer-scale production of ZnO nanowire arrays," *Angew. Chem. Int. Ed.*, vol. 42, pp. 3031-3034, 2003.
[21] D. Buie, M. J. McCann, K. J. Weber, and C. J. Dey, "Full day simulations of anti-reflection coatings for flat plate silicon photovoltaics," *Solar Energy Materials & Solar Cells*, vol. 81, pp. 13-24, 2003.